INTERNATIONAL JOURNAL OF HYDROGEN ENERGY 40 (2015) 1353–1366

Available online at www.sciencedirect.com

ScienceDirect

journal homepage: www.elsevier.com/locate/he

Membrane degradation in PEM water electrolyzer: Numerical modeling and experimental evidence of the influence of temperature and current density

M. Chandesris [a,b,*], V. Médeau [a,b], N. Guillet [a,b], S. Chelghoum [a,b], D. Thoby [a,b], F. Fouda-Onana [a,b]

[a] Univ. Grenoble Alpes F-38000 Grenoble, France
[b] CEA, LITEN, DEHT, F-38054 Grenoble, France

ARTICLE INFO

Article history:
Received 11 September 2014
Received in revised form
20 November 2014
Accepted 21 November 2014
Available online 13 December 2014

Keywords:
PEM water electrolyzer
Numerical modeling
Membrane degradation
Experimental validation
Atmospheric operation

ABSTRACT

In this work, a 1D polymer electrolyte membrane water electrolyzer (PEMWE) model that incorporates chemical degradation of the membrane is developed to study the influence of temperature and current density on the membrane degradation. In the 1D performance model, electronic and ionic transports through the different cell components are considered together with the electrochemical behavior of the anodic and cathodic catalyst layers. The membrane degradation model describes the oxygen cross-over from the anode to the cathode side, the formation of hydrogen peroxyde at the cathode side together with the subsequent formation of radicals via Fenton reactions involving metal-ion impurities and the membrane degradation. The development of the model is supported by specific single cell experiments to both validate the different modeling assumptions and determine some of the physical parameters involved in the performance and degradation models. The single-cell degradation tests confirm that most of the membrane degradation occurs at the cathode side and also show the strong influence of the temperature on the degradation rate. The effect of the current density on the degradation rate is more complex and presents a maximum at quite low current density. This phenomena, observed in the experiments, is well captured by the model. The model is then used to study the time evolution of the membrane thickness. The coupling between the performance and the chemical degradation models allows to capture the acceleration of membrane thinning.

Introduction

Hydrogen may play an important role as an energy carrier in the future. However, as hydrogen does not occur in nature in its elementary or molecular form, hydrogen must be produced. PEM water electrolyzers (PEMWEs) are considered as a viable alternative for generation of hydrogen from renewable energy sources [1]. Indeed they present many advantages over other available WE technologies (simplicity, excellent

* *Corresponding author*. CEA, LITEN/DEHT, 17 rue des Martyrs, 38054 Grenoble Cedex 9, France. Tel.: +33 4 38 78 24 88; fax: +33 4 38 78 41 39.
E-mail address: marion.chandesris@cea.fr (M. Chandesris).
http://dx.doi.org/10.1016/j.ijhydene.2014.11.111

dynamic response to power fluctuations, possibility of compact design, …) making them ideal for operation with intermittent renewable energy sources such as wind and solar power.

Recent impressive progresses have demonstrate the potentiality of PEMWE technology [2–4] and on-going efforts are devoted to search novel solutions to reduce the costs of the systems while maintaining high durability life-time. Reliability and high durability of PEMWE are known for a long time since these systems have been used since the 70's in nuclear submarine for oxygen production with tens of thousands of system hours of operation. However, to reach very reliable devices for military or spatial applications, very expensive components are used: high loading of expensive platinum group metals such as platinum, iridium and ruthenium (among the rarest elements in Earth's crust), thick proton exchange membrane, corrosion resistant metals collectors and bipolar plates, which makes these devices too expensive for usual industrial applications. Nonetheless, recent developments allow several companies to propose very reliable industrial products and to reduce the capital costs of the stacks while maintaining high durability. To pursue that effort, it is necessary to find new component solutions and to evaluate them. While performance can be tested quite rapidly, lifetime estimation is much more difficult to evaluate. Furthermore, in PEM water electrolyzer, degradation mechanisms occur very slowly with a typical characteristic time of thousands of hours, compared to hundreds of hours in PEMFC. Thus, lifetime estimation of the different components requires long and costly experiments, whereas it remains crucial to determine the service life of the electrolyzer. In this context, modeling of degradation mechanisms in PEMWE is a very useful tool to predict the performance of the system over its lifetime depending on the operating conditions (temperature, mission profile, mean current density).

During the last years, research interest has increased around PEMWEs and several performance PEMWE models have been reported in the literature [5–9]. These models are based on thermodynamic principles and Butler–Volmer kinetics and allow for simulating the electrochemical behavior of the electrolyzer depending on the operating conditions (mainly temperature and pressure). More complex models, taking into account mass transfer have also been reported recently. Mass transport limitations are taken into account through a diffusion overvoltage by Marangio et al. [10], while Grigoriev et al. [11] couple electrochemical models and mass transfer models in the current collectors and flow channels to optimize PEMWE for operation at elevated pressures.

Regarding degradation mechanisms in PEMWEs, to our knowledge, no model has been published in the literature. Degradation models for PEMFC can be found in the literature focusing on different mechanisms such as catalysts and catalyst layers degradation [12], cathode catalyst support corrosion [13], membrane degradation [14,15] and limit temperature [16]. However, the PEMFC is not the exact opposite of an electrolysis cell. In PEMWEs, rutile oxydes like IrO^2 and RuO^2 are used as anode catalysts and the membrane is far thicker. Consequently, particular care should be taken when transferring concepts from PEMFC modeling to PEMWE applications. As on PEM fuel cell, there is not a unique cause of degradation. The main sources of performance losses are related to catalysts and catalyst layers degradation, membrane degradation and bipolar plates and current collectors corrosion, however it is quite difficult to isolate the different degradation phenomena. Nevertheless, in PEMWEs, performance decreases and durability restrictions are mostly attributed to membrane pollution or degradation, reason why we will focus on this mechanism. The main idea is to propose a mechanistic model of membrane chemical degradation and to develop this model in a 1D MEA performance model in order to obtain an explicit coupling between membrane degradation and the performance of the electrolyzer. The aim is to provide some insight on the parameters affecting the membrane degradation. The development of the model is supported by specific single cell experiments to both validate the different modeling assumptions and determine the different physical parameters involved in both the performance and the degradation models.

This paper is organized as follows. Section Single cell experimental set-up presents the single cell experimental set-up used in this study and the tested MEAs. In section PEM water electrolyzer performance model, we focus on the proposed 1D MEA performance PEMWE model. The main assumptions are described and the different physical parameters of the components are determined based on the single cell experiments or literature data. The membrane chemical degradation model is then presented in section Membrane degradation model. The degradation model is implemented in the 1D MEA performance model to simulate the macroscopic effects of chemical membrane degradation: fluoride release rate and thinning of the membrane. The obtained results are validated against the experimental data. Finally the model is used to study the time evolution of the membrane thickness and to discuss the impact of different operating conditions on the life-time of the electrolyzer.

Single cell experimental set-up

Chemical membrane degradation at various temperatures and current densities is investigated using a 25 cm^2 single cell set-up. During experiments, only the anode is supplied with deionized water at a constant flow rate of 200 ml h^{-1}. However, water will be collected at both the anode and cathode sides since water crosses the membrane during electrolysis operation, as depicted in Fig. 1. Two MEAs, provided by Johnson Mattey, have been studied. Anode and cathode catalysts loading are almost the same for the two samples: 1.94 mg cm^{-2} of IrO_2 black and 1.19 mg cm^{-2} of Pt black for sample JM 3.4 and 1.99 mg cm^{-2} of IrO_2 black and 1.31 mg cm^{-2} of Pt black for sample JM 3.2 and both MEAs are made of a Nafion N117 membrane. Electrolysis performance of the MEAs is evaluated at beginning of life (BoL) by measuring polarization curves at three different temperatures: 313, 333 and 353 K. The two MEAs have the same performance at BoL. Electrochemical impedance spectroscopy (EIS) are also carried at BoL at the three different temperatures using a high current potentiostat (Bio-Logic Science Instruments SAS, HCP-803, 80 A) at frequencies ranging from 10 kHz to 200 mHz. A stabilization of 2 min is used for each step in order to reach a quasi-

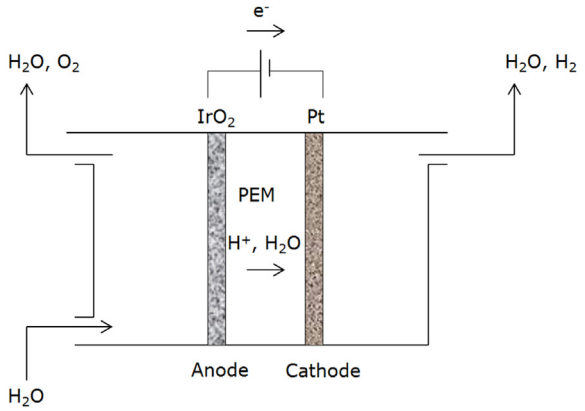

Fig. 1 – Cross-sectional view of the PEM electrolytic cell.

stationary state. The amplitude of the potentiostatic perturbation is chosen in order to verify the assumption of system linearity, while ensuring a sufficient signal/noise ratio. Purely ohmic resistances are then determined by taking high frequency intercepts of Nyquist plots with the real axis, assuming that pure resistance is given at zero phase (Bode plot).

The chemical degradation is characterized by regularly collecting the effluent water of the cell at the anode and at the cathode sides and by measuring the fluoride release rate in the samples using a fluoride selective electrode. A constant current density is applied during approximately 200–300 h, until a sufficient number of water samples is gathered and then the current density is changed. The first MEA (JM 3.4) has been aged at 353 K and the second one (JM 3.2) at 333 K. The fluoride-ion release rate (FRR) is calculated from the flow rate of the collected water and the concentration of F^- ions. The obtained results are presented in Fig. 2. The FRRs from the cathode is obviously far larger than the one at the anode and the temperature has also a strong impact on the membrane degradation, as has been already reported for electrolyzer by LaConti et al. [17]. Increasing the temperature clearly accelerates the membrane degradation. For a given temperature and current density, we can observe some dispersion between the values obtained for the different samples. At 353 K, this dispersion is quite low and does not seem to depend of time. At 333 K, it seems that few samples are needed before obtaining a stabilized value. Despite this stabilization effect, we can still observe a clear influence of the current density on the FRR. The effect of the current density on membrane degradation is summed up Fig. 3, where the sum of the averaged measured FRRs at the anode and at the cathode is presented versus the current density. At both temperatures, the FRR increases as the current density decreases. At 353 K, it reaches a maximum around 0.4 A cm^{-2} and then decreases. At 333 K, the maximum is reached at a lower value, around 0.2 A cm^{-2}.

PEM water electrolyzer performance model

A simple PEM water electrolyzer performance model is developed in this section. The purpose of this model is to

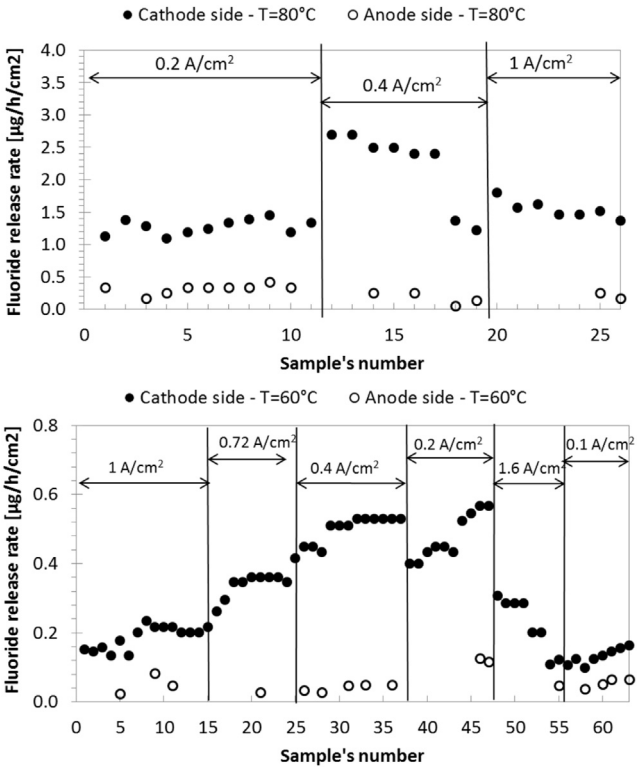

Fig. 2 – Fluoride-ion release rates in the effluent water at the anode and the cathode during tests at 353 and 333 K for different current densities.

correctly account for the electrochemical behavior of the electrolyzer depending on components characteristics and operating conditions to later be able to study the coupling between the membrane degradation and the PEMWE performance. As given by Nernst equation, the reversible potential at each electrode depends on the activity of products and reactants. However, to simplify the performance model, we assume that at first order, the activity of the different products and reactants can be set equal to one in PEM water electrolysis. With this assumption, the modeling of gas and liquid transport in the cell is not needed to account for cell polarization curves. However, given this hypothesis, we

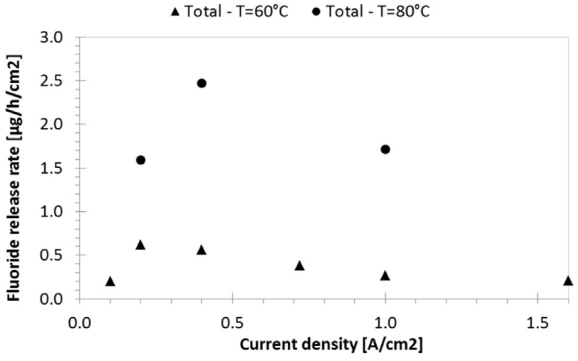

Fig. 3 – Total mean fluoride-ion release rates depending on the current density.

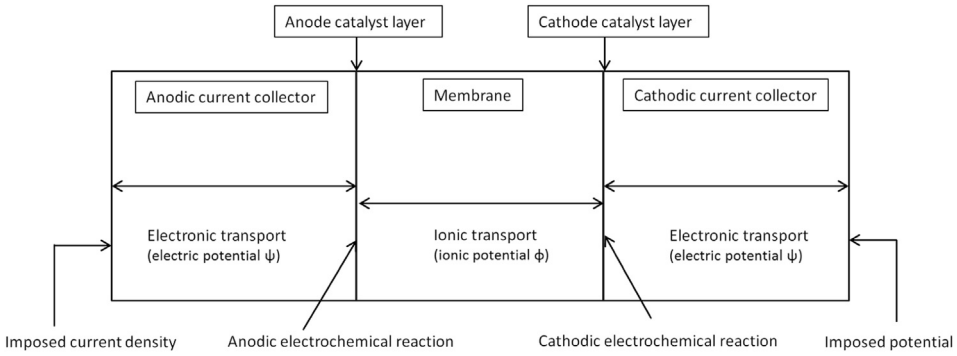

Fig. 4 – Scheme of the computational domain for the 1D MEA performance model including the membrane, the catalyst layers and the current collectors.

acknowledge that pressure effect on I–V curves cannot be captured. This assumption is reasonable for electrolyzer working at atmospheric pressure, but could not be used when studying electrolyzers operating at elevated pressure. It is also assumed that the temperature is uniform inside the cell. Given, these assumptions, the current-potential relationship of the cell can be obtained by modeling the electrochemical behavior of the anode and cathode catalyst layers, the ionic potential in the membrane and the electric potential in the two current collectors as presented in Fig. 4 and detailed in the next section.

Physical model

The different components considered in this simple 1D MEA performance model are the solid polymer electrolyte membrane, the anodic and cathodic current collectors, the anode and cathode catalyst layers, which are considered here as interfaces, as depicted Fig. 4. The different domains are modeled individually and connected through appropriate boundary conditions. The aim of this model is to determine the potential difference of the cell given the applied current density, the components characteristics and the operating conditions. The MEA dimensions and physical constants used in the model are listed in Table 3.

Membrane. In PEM water electrolyzers, one of the dominant losses is the ionic loss caused by the resistance to the proton transport through the polymeric membrane. At steady state, the divergence of the current density, i, in the membrane is zero and the current density can be related to the ionic potential ϕ via ohm's law:

$$\nabla \cdot i = 0 \tag{1}$$

$$i = -\kappa \nabla \phi \tag{2}$$

Table 1 – Half-cell reactions and associated energy for a PEM water electrolysis cell.

	Half-cell reaction	ΔH (kJ mol^{-1})	ΔS (J mol^{-1} K^{-1})
Anode	$2H_2O \rightarrow 4H^+ + 4e^- + O_2$	6229.6	326.36
Cathode	$2H^+ + 2e^- \rightarrow H_2$	−2829	−0.104

where κ is the conductivity of the electrolyte. This conductivity depends on the temperature T and on the water content λ.

Anodic and cathodic current collectors. To ensure good current collections, materials must have a good electronic conductivity. Furthermore, to favor the distribution of the water and the evacuation of produced gas bubbles, the current collectors are porous with good mechanical resistance. In PEMWEs, anodic potentials are so high (typically comprised between 1.6 and 2 V) that carbon-based and most metal-based current collectors cannot be used due to their rapid oxidation. Thus, at the anode side, porous current collectors made of sintered titanium particles are usually used, whereas standard carbon-based gas diffusion layer are used at the cathode side. The variation of the electric potential ψ across the two current collectors is modeled using the conservation of charge and Ohm's law:

$$\nabla \cdot i = 0 \tag{3}$$

$$i = -\sigma \nabla \psi \tag{4}$$

where σ, which is supposed to be isotropic, is the effective electronic conductivity of the porous collectors. In the following, the electronic conductivity of the anodic and cathodic current collectors are noted respectively σ_A and σ_C.

Anode and cathode catalyst layers. Assuming only charge transfer limitations and no transport limitations, the Butler-Volmer expression is used to relate the current density to the activation overpotential at each electrode. At the anode, water is dissociated into oxygen, proton and electron via the following reaction:

$$H_2O \rightarrow 2H^+ + 2e^- + \frac{1}{2}O_2 \tag{5}$$

At the cathode, protons are reduced to form hydrogen:

$$2H^+ + 2e^- \rightarrow H_2 \tag{6}$$

At each electrode, the Buttler-Volmer expression reads:

$$i = i_{0j}\gamma_j \left[\exp\left(\frac{\alpha_j z F}{RT} \eta_j \right) - \exp\left(-\frac{(1-\alpha_j) z F}{RT} \eta_j \right) \right] \tag{7}$$

where the subscript j is equal to A at the anodic side and C at the cathodic side, at each electrode i_{0j} is the exchange current

Table 2 – Kinetic parameters for the anode activation overpotential.

Temperature (K)	Tafel slope (mV)	α_A	$i_{0A}\gamma_A$ (A/m^2)
353	54.4	0.648	2.36×10^{-2}
333	51.5	0.650	5.94×10^{-3}
313	48.0	0.655	1.0×10^{-3}

density, γ_j is the electrochemical active surface area per geometric surface, α_j is the charge transfer coefficient, z is the stoichiometric coefficient for transferred electrons in the global semi reactions (z = 2 in water electrolysis), F is the Faraday's constant and η_j is the overpotential.

The value of the exchange current density, i_{0j} depends on the used electro-catalyst, the temperature, the electrode morphology and other factors. In the present work, assuming that the activity of the different products and reactants can be set equal to one, the exchange current density is modeled in the following way:

$$i_{0j} = zFk_{0j}T\exp\left(-\frac{A_{0j}}{RT}\right) \quad (8)$$

where A_{0j} is the activation energy and k_{0j} the rate parameter per unit surface of the anodic ($j = A$) or cathodic ($j = C$) reaction. At both electrodes, the overpotential is obtained from the following relation:

Table 3 – Geometrical and physical parameters used in the performance model.

Parameters	Symbol	Value (unit)
Geometrical parameters:		
Membrane thickness	e_M	178 (μm)
Anodic current collector thickness	e_A	1.4 (mm)
Cathodic current collector thickness	e_C	235 (μm)
Physical constants:		
Faraday's constant	F	96,485 (C mol^{-1})
Gas constant	R	8.314 (J K^{-1} mol^{-1})
Physical parameters of the performance model:		
Electronic conductivity of the anodic current collector	σ_A	13,700 (S m^{-1})
Electronic conductivity of the cathodic current collector	σ_C	46 (S m^{-1})
Number of water molecules per sulfonate site	λ	16
Anodic rugosity factor	γ_A	150 (m^2/m^2)
Cathodic rugosity factor	γ_C	150 (m^2/m^2)
Anodic charge transfer coefficient	α_A	0.65
Cathodic charge transfer coefficient	α_C	0.51
Anodic activation energy	A_{0A}	62,836 (J mol^{-1})
Cathodic activation energy	A_{0C}	24,359 (J mol^{-1})
Anodic rate parameter	k_{0A}	4.63×10^{-3} (mol/K/s/m^2)
Cathodic rate parameter	k_{0C}	1.0×10^{-2} mol/K/s/m^2

$$\eta_j = \psi - \phi - E^j_{rev} \quad (9)$$

where E^j_{rev} is the reversible potential of the j electrode. This reversible potential is evaluated at each electrode using the Nernst equation:

$$E_{rev} = \frac{-\Delta G}{nF} + \frac{RT}{nF}\ln\left(\prod_i a_i^{\nu_i}\right) \quad (10)$$

where ν_i is the stochiometric coefficient of the i-constituent of the reaction. The variation of the total free Gibbs energy is related to the variation of enthalpy and entropy:

$$\Delta G = \Delta H - T\Delta S \quad (11)$$

The enthalpy and entropy variations for each half cell reactions are taken from the work of Lampinen and Fomino [18] and are presented in Table 1.

Physical parameters determination

The results of the performance model directly depend on the physical properties of the different components of the tested MEA: thickness and ionic conductivity of the membrane, thickness and electronic conductivity of the two current collectors, electrochemical properties of the catalyst layers. These physical properties are determined based on the results of the single cell experiments and literature data.

To determine the catalyst properties, we use the experimental results obtained at beginning of life (BoL) with the polarization curves and the electrochemical impedance spectra at the three different temperatures. The measured potential of the cell is the sum of the reversible potential of each electrode, of the anodic and cathodic overpotentials and of the ohmic losses:

$$U = E^A_{rev} + E^C_{rev} + \eta_A + \eta_C + R_{ohm}i \quad (12)$$

where R_{ohm} is the total ohmic resistance of the cell. The reversible potential E^j_{rev} is determined at each electrode using the Nernst equation (10) and assuming that the activity of the products and reactants is equal to one, which is a reasonalble hypothesis for PEMWE working at atmospheric pressure. The total ohmic resistance of the cell has been determined experimentally at three different temperatures from the EIS measurements. Neglecting contact resistance, it can be expressed as the sum of the ohmic losses in the membrane and in the two porous current collectors:

$$R_{ohm} = \frac{e_M}{\kappa} + \frac{e_A}{\sigma_A} + \frac{e_C}{\sigma_C} \quad (13)$$

The specific electric resistance of the anodic titanium current collector can be estimated around 7.3 mOhm cm based on the work of Grigoriev et al. [11], which corresponds to an electronic conductivity of the anodic current collector of σ_A = 13,700 S/m. The electronic conductivity of the cathodic carbon current collector is evaluated around σ_C = 46 S/m. Regarding the electrolyte conductivity, the empirical law of Springer et al. [19] is used to determine the ionic conductivity of the membrane:

$$\kappa_{303} = 0.5139\lambda - 0.326 \tag{14}$$

$$\kappa(T) = \kappa_{303} \exp\left[1268\left(\frac{1}{303} - \frac{1}{T}\right)\right] \tag{15}$$

The water content of the membrane, λ, is a crucial issue on PEM fuel cells. During PEMFC operation, water is carried into the cell via humidified gas stream and the membrane is equilibrated with water vapor. In this case, water uptake decreases with increasing temperature. In the case of PEM water electrolyzers, the membrane can be considered as fully saturated with liquid water and water uptake from liquid water differs from water vapor. In this case λ strongly depends on the pretreatment of the membrane [20] and is known to be in the range 14–21. Assuming $\lambda = 16$, we recover using equation (13) the measured ohmic resistance and its dependence with temperature as can be seen in Fig. 5.

The sum of the anodic and cathodic overpotentials is given by:

$$\eta_A + \eta_C = U - R_{ohm} i - E^A_{rev} - E^C_{rev} \tag{16}$$

Assuming no transport limitations, the Butler-Volmer expression (7) is used at both electrodes to relate the overpotential, η_j, to the exchange current density, i_{0j}. Although during the global reaction each electrode has its own contribution to the activation overpotential, this contribution is not symmetric. The values of the exchange current density at the anode are much lower. In order to estimate the electrochemical parameters, in a first step, we neglect the cathode contribution to the activation overpotentials. Furthermore, it can be assumed that one of the branches in the Butler-Volmer expression will dominate during operation (oxidation at the anode and reduction at the cathode). Therefore, the anodic overpotential can be related to the exchange current density using the following expression, for parameters determination:

$$\eta_A \simeq \frac{RT}{\alpha_A zF} \ln\left(\frac{i}{i_{0A}\gamma_A}\right) \tag{17}$$

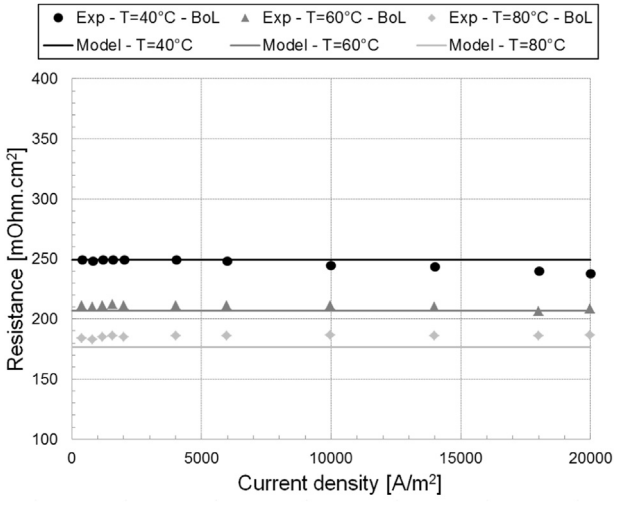

Fig. 5 – Total resistance of the cell as a function of temperature and current density. Comparison between model and experiment.

Fig. 6 presents the evolution of the current density with the overpotential using logarithmic scale for the three different studied temperatures. The corresponding Tafel's slopes and the anodic exchange current density i_{0A} times the rugosity γ_A are presented in Table 2. The values obtained at 80° C (353 K) are similar to those presented by Ito et al. [21], who obtain exhange current density values between 0.85×10^{-2} and 1.70×10^{-2} A/m^2 at 80° C. From the Tafel slope's results, the anodic transfer coefficient is estimated to be around $\alpha_A = 0.65$, which is a value close to the one obtained by Rozain [22] for other PEMWE's MEA based on iridium oxyde ($\alpha_A = 0.63$). Regarding the rugosity factors, γ_j, since we had no mean to estimate them, we used as in Ref. [5] a value of 150 at both the anode and the cathode. Using the value of the exchange current density at three different temperatures and the rugosity factors, the anodic activation energy and the anodic rate parameter can be estimated. We obtain $A_{0A} = 62836$ J/mol and $k_{0A} = 4.63 \times 10^{-3}$ mol/K/s/m^2. The later value could be up-dated without changing the overall results if obtaining experimental data for the anodic rugosity factor.

Regarding the evaluation of the electro–chemical parameters at the cathode side, it is trickier since this overpotential is almost negligible, but at the same time, the consequences are less important. We assume that the cathodic transfer coefficient and the cathodic activation energy are the same as the one obtained on a previous work obtained for platinum catalyst for PEMFC: $\alpha_C = 0.51$ and $A_{0C} = 24{,}359$ J/mol. The value of the cathodic rate parameter, k_{0C} is then fitted to the experimental results. We obtain $k_{0C} = 1.0 \times 10^{-2}$ mol/K/s/m^2. This value could be updated if we have access to individual overpotentials at each electrode.

A summary of all the parameters determined in this section is presented Table 3. As can be seen on Fig. 7, the present performance model is able to capture the polarization curves obtained experimentally for the three different temperatures for the first MEA and similar results are obtained for the second one. In particular, the behavior at low current density, characteristic of the electrochemical model, is well captured as can be seen using a logarithmic scale on Fig. 7.

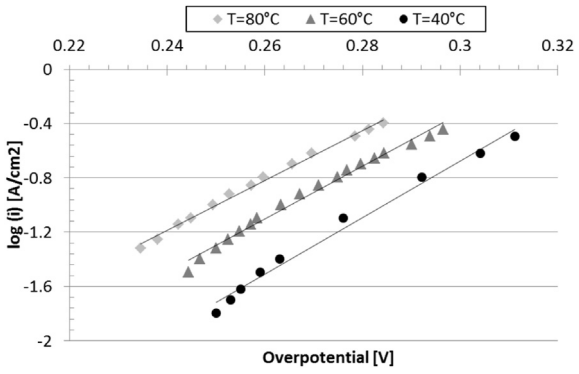

Fig. 6 – Evolution of the current density with the overpotential for the three different temperatures.

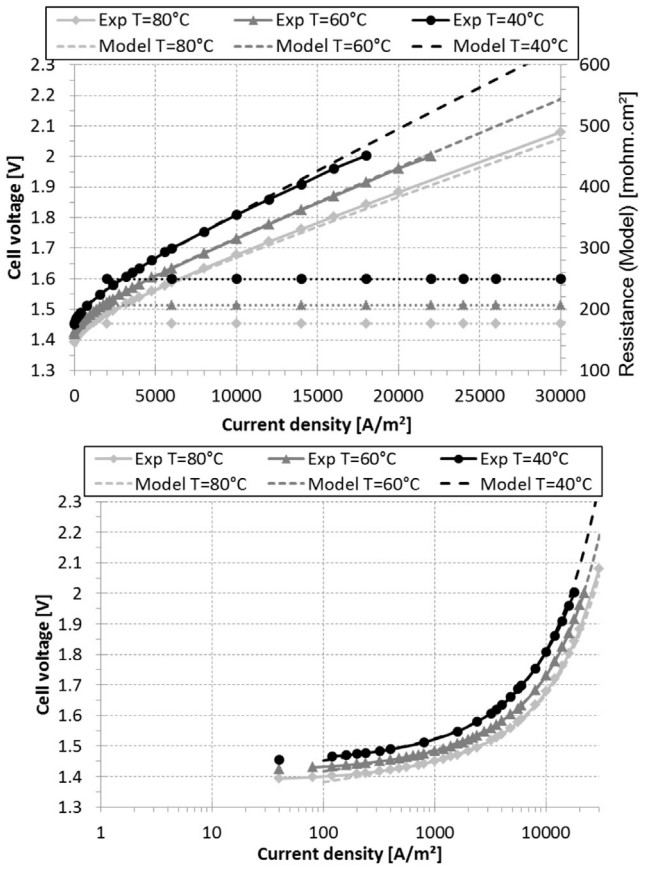

Fig. 7 – Experimental (JM 3.4) and simulated cell potentials at different current density and temperature. The behavior at low current density, characteristic of the electrochemical model, is displayed on the bottom using a log scale.

Membrane degradation model

In PEMFC's, membrane chemical degradation is reported to occur through the following scenario [14,15,23]: hydrogen peroxyde (H_2 O_2) electrochemical formation via the two-electron oxygen reduction reaction in the catalyst layers, diffusion of H_2 O_2 into the membrane, decomposition into free radicals via Fenton's reaction mechanism in the presence of ferrous ions and finally attack of the membrane by the free radicals.

For PEMFC, peroxyl radical formation and membrane degradation are reported to occur on either side of the MEA, depending on the operating mode [17,24].

Regarding PEMWE, one of the most complete studies that gives evidence of membrane degradation was conducted at PSI in the 1990's [25] where substantial thinning of the membranes has been detected. Regarding the dissolution process, the ion exchange capacity measurements on thinned membranes reveal that the composition of the remaining polymer is not changed with respect to ionic groups: the degradation mechanism does not involve preferential attack on the ion exchange groups. Furthermore, complementary experiments indicated that the membrane degrading reaction can be localized on the cathode side of the cell. The interfaces with the anode as well as the bulk of the membrane were quite less affected [17,25]. In the present study, as reported in section Single cell experimental set-up, we have observed a non negligible fluoride release only on the cathode side, which also support the hypothesis that membrane degrading reactions occur mainly at the cathode side for PEMWE. The following scenario will thus be considered in the model: oxygen cross-over from the anode to the cathode side through the membrane, production of hydrogen peroxide (H_2O_2) at the cathode side, formation of free radicals that attack the membrane on the surface without altering the transport properties of the membrane, leading to fluoride release and thinning of the membrane.

Model description

Gas cross-over. One of the role of the membrane is the separation of gases between the anode and the cathode side. However, Nafion cannot prevent the oxygen and hydrogen to permeate between the electrodes. This gas cross-over through the membrane appears to be mainly due to two mechanisms. First, as oxygen (resp. hydrogen) is present under gas form only at the anode (resp. cathode), a concentration gradient appears, once the gases are dissolved in the ionomer of the membrane. This concentration gradient induces an oxygen flux from the anode to the cathode and a hydrogen flux from the cathode to the anode via a diffusive process. Furthermore, water is crossing the membrane from the anode to the cathode due to both electro-osmotic phenomenon and water diffusion. Since part of the produced gas gets soluble in the water, it can be assumed that it is convectively carried through the membrane by this water flow. Thus, the transport of dissolved gases in the membrane can be expressed as:

$$v_{H_2O} \cdot \nabla c_i = \nabla \cdot D_i \nabla c_i \quad (18)$$

where c_i is the concentration and D_i is the diffusion coefficient in Nafion of solved species i and v_{H_2O} is the water velocity inside the membrane.

In each current collector j, the partial pressure P_i^j of specie i can be assumed to be constant. Assuming that the solubility coefficient of gases in the membrane and in the water are almost the same [20], the concentration of solved species i at the membrane boundaries is the same as the one in the water present in the anodic and cathodic chambers. This concentration is proportional to the partial pressure:

$$c_i^j = S_i P_i^j \quad (19)$$

where c_i^j is the concentration of species i at the j frontier of the membrane, P_i^j is the partial pressure of species i in the current collector j and S_i is the solubility of species i in water. This gas cross-over model is described shematically Fig. 8.

The values for the solubility and diffusion coefficients are chosen among a large base of experimentally given laws [20,26,27]. Those laws are always temperature dependent and sometimes depend also on the water uptake of the membrane. Furthermore, it should be noted that a quite large dispersion of the obtained values can be observed. The laws retained for this study are presented in Table 4. They correspond to medium permeation behavior. To get a H_2

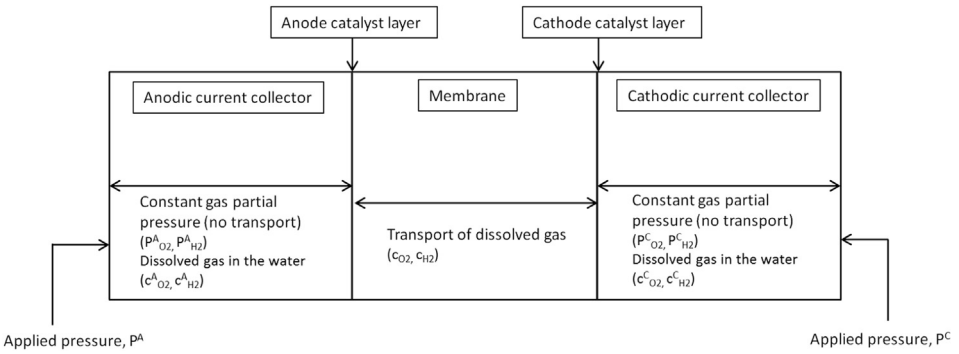

Fig. 8 – Scheme of the computational domain and assumptions for the gaz cross-over model.

permeation coefficient ($\mathscr{P}_{H_2} = S_{H_2} D_{H_2}$ the notation $\mathscr{P}$ is used to avoid confusion with the pressure), two times higher than the one given for O_2, the diffusion coefficient of H_2 reported in Ref. [28] has been arbitrarily multiplied by 3, while the solubility coefficient reported in Ref. [29] has been divided by ω, where ω is the water uptake of the membrane in weight percent of water, $\omega = \lambda M_{H_2O}/EW$, M_{H_2O} being the molar mass of water and EW is the equivalent weight (weight of dry Nafion per mol of sulfonate acid groups), which is equal to 1.1 kg/mol of Nafion.

The water flow through the membrane is the result of a combination between eletro-osmose and water diffusion, the resulting net flow going exclusively from the anode to the cathode side. In the present model, this law is obtained from the experimental results, based on the collected water at the cathode side of the electrolyzer:

$$Q^t_{H_2O} = (-0.332\ \log I + 5.59) Q^c_{H_2O} \tag{20}$$

where I is the current density, $Q^t_{H_2O}$ is the transfered water flow and $Q^c_{H_2O}$ is the consumed water flow, which is equal to:

$$Q^c_{H_2O} = \frac{M_{H_2O} I S}{2F\rho_{H_2O}} \tag{21}$$

where S is the membrane's surface. The water velocity through the membrane is thus simply given by:

$$v_{H_2O} = \frac{Q^t_{H_2O}}{S} \tag{22}$$

In each current collector, the partial pressure of oxygen and hydrogen are assumed constant. To determine their value, first the mass balance of fluxes is written for O_2 and H_2 on both side of the membrane. At the cathode side:

$$j^{perm}_{O_2} - j^{reac}_{O_2} - j^{gC}_{O_2} - j^{wC}_{O_2} = 0 \tag{23}$$

$$-j^{perm}_{H_2} + S_{H_2} - j^{gC}_{H_2} - j^{wC}_{H_2} = 0 \tag{24}$$

At the anode side:

$$j^{perm}_{H_2} - j^{reac}_{H_2} - j^{gA}_{H_2} - j^{wA}_{H_2} = 0 \tag{25}$$

$$-j^{perm}_{O_2} + S_{O_2} - j^{gA}_{O_2} - j^{wA}_{O_2} = 0 \tag{26}$$

where $S_i = i/(nF)$ is the source term due to the main reaction of the electrolyzer ($n = 2$ for H_2 and 4 for O_2), j^{gj}_i is the gaseous flow leaving the cell on side j, j^{perm}_i is the permeation flux through the membrane determined from the transport of dissolved gas through the membrane (Eq. (18)), j^{wj}_i is the flux of gas i leaving the cell on side j through dissolution into water, $j^{wj}_i = v^j_{H_2O} c^j_i$, and j^{reac}_i is the molar flux of permeated gaz consumed by side reactions. In this work, only the side reactions involving O_2 at the cathode side will be considered through peroxyde formation and free radicals formation. The partial pressure of gases is then deduced from the gas flux balance:

$$P^j_i = x^j_i P^j = \frac{j^{gj}_i}{\sum_i j^{gj}_i} P^j \tag{27}$$

where x^j_i is the molar fraction of gas i at side j and P^j is the total pressure at side j of the electrolyzer. The obtained molar fractions for O_2 on the cathode side, respectively H_2 on the anode side, in function of the current density are presented in Fig. 9 for different temperatures. The expected decrease with the current density is recovered. At very low current density, a very high molar percentage is observed due to the fact that a smaller amount of the other gas is produced. A strong difference between O_2 and H_2 molar fractions can be observed. This is due to the fact that the permeation coefficient and the

Table 4 – O_2 and H_2 solubility and diffusivity coefficients.

Parameter (unit)	O_2	H_2
S_i (mol Pa^{-1} m^{-3})	$1.62 \times 10^{-6} \exp(603/T)$ [30]	$1/\left(\omega \cdot 1.09 \times 10^5 \exp\left(\frac{77}{T}\right)\right)$ [29]
D_i (m^2 s^{-1})	$4.2 \times 10^{-6} \exp\left(-\frac{-18380}{RT}\right)$ [31]	$1.23 \times 10^{-6} \exp\left(-\frac{-2602}{T}\right)$ [28]

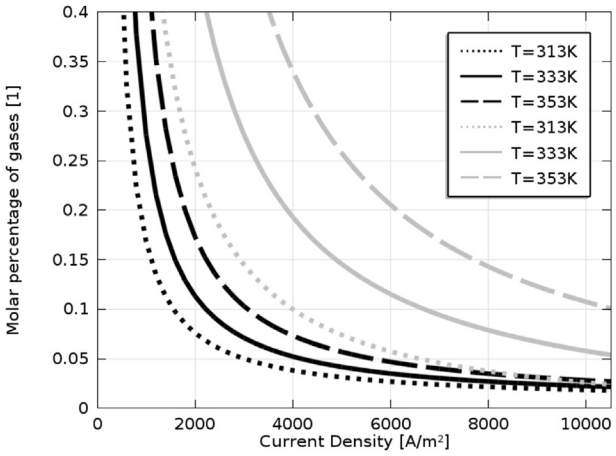

Fig. 9 – Comparison between O_2 (black) and H_2 (gray) molar percentages respectively at the cathodic and anodic sides at temperature 313 K, 333 K and 353 K.

source term are greater for H_2. The model is also as expected strongly temperature dependent.

Hydrogen peroxyde formation. Once arrived at the cathode side, oxygen is involved into oxygen reduction reactions (ORR) which can occur through a 2 or a 4-electron exchange reaction. The cathode side is at very low potential (< 0 V vs. SHE), as hydrogen evolution reaction occurs at the platinum electroactive sites. At potential lower than 0.4 V, ORR is considered to predominantly occurs via H_2O_2 formation pathway [32] and one can neglect water recombination:

$$O_2 + 2H^+ + 2e^- \rightarrow H_2O_2 \tag{28}$$

The electrochemical formation rate of H_2O_2 is modeled using a simple order kinetic law and assuming that the reverse reaction is negligible [33]:

$$R_1 = k_1 c_{O_2} c_{H^+}^2 \tag{29}$$

The kinetic constant per unit of electrochemically active surface, k_1, is given by Ref. [33]:

$$k_1 = k_1^0 \exp\left(\frac{-\alpha_{H_2O_2} F}{RT^0}\eta_{2e}\right) = k_{1_0}^0 \exp\left(\frac{-A_{H_2O_2}}{RT}\right)\exp\left(\frac{-\alpha_{H_2O_2} F}{RT^0}\eta_{2e}\right) \tag{30}$$

$\alpha_{H_2O_2}$ is the transfer coefficient associated to this electrochemical reaction and is assumed to be equal to 0.5. η_{2e} is the cathodic overpotential related to the 2-electron oxygen reduction reaction, the equilibrium potential being taken equal to 0.695 V vs SHE, $A_{H_2O_2}$ is the activation energy of the electrochemical reaction. Anderson and Albu [34] reports an activation energy of 42,450 J/mol on Pt/C with Nafion for the electrolyte, in agreement with values by Sethuraman et al. [33] and Wong and Kjeang [15]. Sethuraman et al. [33] report a value of 2.56×10^{-5} cm^7 mol^{-2} s^{-1} for k_1^0 at 298 K, which leads to $k_{1_0}^0 = 7.068 \times 10^2$ m^7 mol^{-2} s^{-1}. The formation rate within the volume of the catalyst layers is then simply given by Ref. $v_1 = \gamma_C R_1 / e_{clC}$ where e_{clC} is the thickness of the cathodic catalyst layer and γ_C is the rugosity of the cathode electrode.

The proton concentration, c_{H^+}, is calculated using the density and equivalent weight of the ionomer in the cathodic catalyst layer [15,33]:

$$c_{H^+} = \frac{\rho_M}{EW} = \frac{1980 + 32.4\lambda}{(1 + 0.00648\lambda)EW} \tag{31}$$

where ρ_M is the humidity-dependent density of the polymer.

Radical formation. The decomposition of hydrogen peroxyde into hydroxyl and hydroperoxyl ($HO^\bullet$ and $HOO^\bullet$) radicals has already been widely studied. In the present study, we consider decomposition of hydrogen peroxyde with and without the presence of Fenton active metal ions (in our case Fe^{2+}). The direct reaction (homolysis of H_2O_2) is kinetically very low compared to those in presence of ferrous ions. Those ferrous ions could arise from the manufacturing process, be injected into the system via the metallic pipes supplying the water or come from the corrosion of the end plates. The chemical reactions involving the radicals and their associated kinetic constants are taken from the work of Gubler et al. [35] and are presented in Table 5. Reactions 2–4 involve radicals formation from decomposition of hydrogen peroxyde with and without the presence of ferrous ions. Reactions 5 to 9 correspond to parasite consumption of the radicals and reaction 10 corresponds to the $HO^\bullet$ radical attack of the membrane. All the kinetic constants are given at 298 K as reported in Gubler et al. [35], except for the kinetic constant of reaction 3, which is an important reaction and for which its temperature dependency has been found in the literature [36]. The reaction rate of the different chemical reactions, v_i ($i = 2–10$), are all assumed to

Table 5 – Overview of the reactions involving free radicals and their associated kinetic constants.

#	Reaction	Rate constant
2	$H_2O_2 \rightarrow 2HO^\bullet$	$k_2 = 1.2 \times 10^{-7} (s^{-1})$
3	$H_2O_2 + Fe^{2+} \rightarrow Fe^{3+} + HO^\bullet + HO^-$	$k_3 = 1.05 \times 10^8 \exp(-9460/RT)$ (l.mol^{-1} s^{-1})
4	$H_2O_2 + Fe^{3+} \rightarrow Fe^{2+} + HOO^\bullet + H^+$	$k_4 = 4 \times 10^{-5}$ (l mol^{-1} s^{-1})
5	$HO^\bullet + Fe^{2+} \rightarrow HO^- + Fe^{3+}$	$k_5 = 2.3 \times 10^8$ (l mol^{-1} s^{-1})
6	$HO^\bullet + H_2O_2 \rightarrow HOO^\bullet + H_2O$	$k_6 = 2.7 \times 10^7$ (l mol^{-1} s^{-1})
7	$HO^\bullet + O_2 \rightarrow HOO^\bullet + H_2O$	$k_7 = 1.2 \times 10^{10}$ (l mol^{-1} s^{-1})
8	$HOO^\bullet + Fe^{3+} \rightarrow Fe^{2+} + O_2 + H^+$	$k_8 = 2 \times 10^4$ (l mol^{-1} s^{-1})
9	$HOO^\bullet + Fe^{2+} + H^+ \rightarrow Fe^{3+} + H_2O_2$	$k_9 = 1.2 \times 10^6$ (l mol^{-1} s^{-1})
10	$HO^\bullet + R_f - CF_2 - COOH \rightarrow$ products	$k_{10} \leq 10^6$ (l mol^{-1} s^{-1})

follow a simple order kinetic law regarding the reagents concentrations, c_j:

$$v_i = k_i \prod_j c_j \tag{32}$$

The time evolution of the concentration of the different species present in the cathodic catalyst layer (H_2O_2, $HO^{\bullet}$, $HOO^{\bullet}$, Fe^{2+} and Fe^{3+}) is obtained by writing the molar mass balance equation of each species over the thickness of the cathodic catalyst layer, which is modeled here as an interface:

$$\frac{dc_j}{dt} = \sum_i \left(-\text{sign}(\nu_{ji})\delta_{ij} \right) v_i + \frac{j_j^{in}}{e_{clC}} - \frac{j_j^{out}}{e_{clC}} \tag{33}$$

where ν_{ji} is the stochiometric coefficient of the j-constituent involved in reaction i, δ_{ij} is equal to one when specie j is involved in reaction i and zero otherwise and j_j^{in} (resp. j_j^{out}) is the molar flux per unit surface of specie j entering (resp.leaving) the cathodic catalyst layer. The incoming molar fluxes, j_j^{in} are set equal to zero for all the species if not stated otherwise and the leaving molar fluxes, j_j^{out}, correspond to the convection by water of the different species out of the cathodic catalyst layer, $j_j^{out} = v_{H_2O} c_j$. Since only steady-state solutions are looked for, the initial concentrations are taken equal to previous computed value to facilitate the convergence of the simulation.

Source of metallic ions. The presence of metallic ions has been widely discussed in both PEMFC and electrolyzer. Those ions are mainly assumed to come from corrosion of stainless steel parts and pipes supplying the system in water. Those metallic ions are reported to be mostly Fe^{2+} ions (more than 70% of ions produced [37,38]) and are usually assumed to be in the order of magnitude of a few ppm. The source of metallic ion is an important parameter of the model, as the final degradation rate appears to be almost proportional to it. In absence of experimental data, the source term will be fitted in order to correspond to expected values of Fe^{2+} concentration and overall degradation. Furthermore, source term of Fe^{2+} can be implemented in several ways, listed below in order of complexity:

- Constant source term. A volumic constant source term is added in the molar balance of Fe^{2+}. This constant source term does not depend on the temperature or the current density.
- Imposed inlet concentration. The concentration at the inlet (anodic side) of the electrolyzer is assumed to be constant and equal to a few ppm. This leads to an incoming flux of Fe^{2+} which depends on the transfered water and is thus current density dependent.
- Condition dependent source term. As reported by Yang et al. [38], the corrosion rate depends on the temperature, pH, fluoride ion concentration and potential. Based on the results of Yang et al. [38], the following linear dependence of the source term with the temperature will be tested:

$$S_{Fe^{2+}} = S_{Fe^{2+}}^{353\,K} \frac{T - 290}{353 - 290} \tag{34}$$

where $S_{Fe^{2+}}^{353\,K}$ is the constant source term determined at 353 K.

Membrane attack mechanism. The mechanisms by which the Nafion membranes are attacked have been widely discussed and although some of the reaction pathways have been identified others remain hypothetical. Therefore, no clear kinetic constant is related to the "overall" degradation mechanism of the membrane modeled here by the reaction #10 in Table 5. Nevertheless a value around $10^5/10^6$ s^{-1} can be expected for k_{10} [35]. Another question is the impact, in term of membrane degradation and fluoride release of reaction # 10. This reaction is assumed to cut the side chains. The impact on the membrane is strongly dependent of the fact that an entire chain is cut or just a part of it, or even several chains all at one. The chemical composition of Nafion is $[(C_2{-}F_4)x{-}(C_2F_3)]{-}(C_3F_6O)_2{-}(C_2F_4O_4H)$, the $(C_2{-}F_4)x{-}(C_2F_3)$ representing the backbone and the rest being the side-chain. X is on average equal to 6.5, thus the release of an entire side-chain plus the backbone corresponds to 45 atoms of Fluor. As explained by Wong and Kjeang [15], the degradation reaction uses one $HO^{\bullet}$ in order to cut the $(C_2F_4O_4H)$ part, three $HO^{\bullet}$ for $(C_3F_6O)_2$ and one $HO^{\bullet}$ to cut the backbone in half, releasing two $(CF_2)_x$/COOH parts. Those two chains then need both x/2 $HO^{\bullet}$ for a complete unzipping. Thus, globally, the mechanism uses 12.5 $HO^{\bullet}$ for the entire unzipping of the side-chain plus corresponding backbone. As a consequence, the fluor release rate will be taken equal to 3.6 times the kinetic rate of the 10th reaction, $v_{fluor} = 3.6 v_{10}$.

Results and discussion

Fig. 10 presents a comparison between the experimental and the simulated fluoride release rates obtained at 353 K. These simulations results are obtained using a constant source term of Fe^{2+} fitted to 9×10^{-2} mol/m^3/s and ±20% variations around this value are also displayed for comparison. The model is able to capture the current density effect on the Fluoride release rate. At very low current

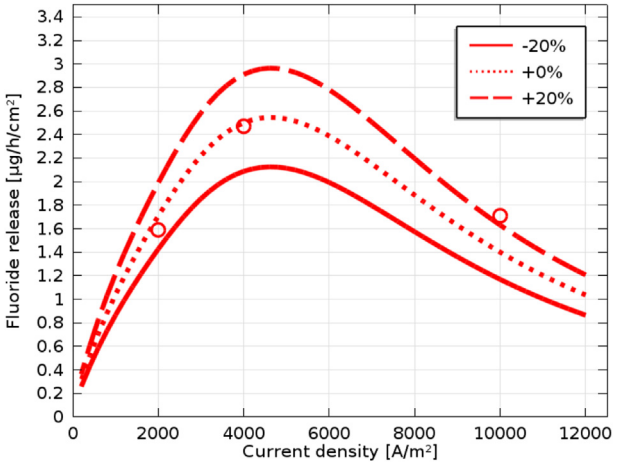

Fig. 10 – Fluoride release at 353 K in µg/h/cm^2 with comparison to experimental points. Modeling results are obtained with a constant source term of Fe^{2+} of 9×10^{-2} mol/m^3/s. ±20% variations around this value are also displayed for comparison.

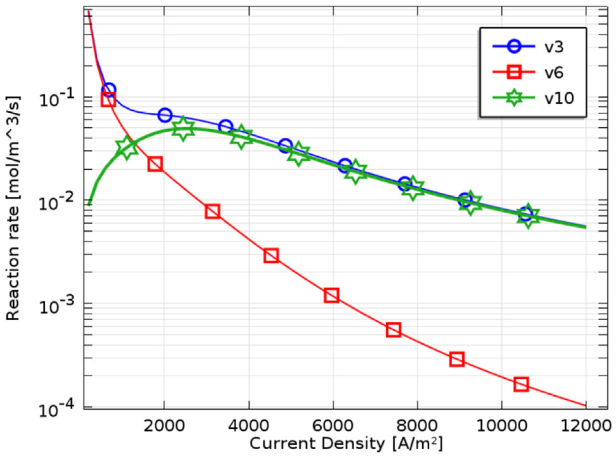

Fig. 11 – Reaction rates of reaction 3, 6 and 10 at 353 K.

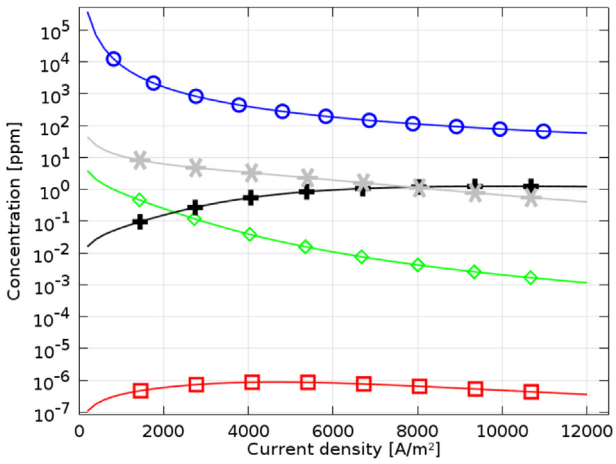

Fig. 12 – Current density dependency of species concentration at 353 K. Blue (circle): H_2O_2, grey (star): Fe^{3+}, black (cross): Fe^{2+}, green (diamond): $HOO^{\cdot}$, red (squarre). $HO^{\cdot}$. (For interpretation of the references to color in this figure legend, the reader is referred to the web version of this article.)

density, the degradation rate is low, then it increases as the current density increases to reach a maximum at quite low current density and then decreases. At high current density, we were expecting a decrease in the Fluoride release since the molar percentage of oxygen decreases and thus the peroxyde formation. However, at low current density, the observed behavior was not expected. To understand the overall shape of the curve, the reaction rates of reactions 3, 6 and 10 are displayed Fig. 11. Reaction 3 is the main source of hydroxyl radicals $HO^{\cdot}$ along with reaction 2 whose order of magnitude is negligible in those conditions whereas reactions 6 and 10 are the two main consumption reactions for $HO^{\cdot}$ (along with reactions 5 and 7). Thus, when neglecting minor reactions, we have $\upsilon_3 = \upsilon_6 + \upsilon_{10}$, where υ_{10} is the membrane degradation reaction rate. As can be seen in Fig. 11, at very low current densities, reaction 6 counts for an important part of the radicals consumption, up to almost all the radicals consumption under 1000 A/m^2. Indeed, as the concentration of H_2O_2 becomes important at very low currents, the sixth reaction rate becomes dominant compared with the reaction rate of the membrane degradation and thus consumes almost all the $HO^{\cdot}$, explaining the lower fluoride release encountered at low current densities.

Fig. 12 presents the concentration of the different species in ppm when the electrolyzer is operating at 353 K. As expected, the free radicals are very low as they are very reactive and stabilize around 10^{-6} to 10^{-7} ppm. The Fe^{2+} ions, highly consumed at low current density through reaction 3, stabilize around a few ppm for medium to high currents. Fe^{3+} ions and $HOO^{\cdot}$ radicals, while produced in important quantities for low current through reactions 6 and 3 respectively, are consumed with lower reactions rates and thus vary greatly from 10^2 to 10^{-1} and 10 to 10^{-3} respectively. Finally, H_2O_2, while mainly bounded between 10 and 10^2 ppm, is largely predominant under 2000 A/m^2, reaching up to 10^5 ppm.

As previously pointed out, the source term of metallic ions is a significant parameter of the model and the fluoride release and degradation rates are almost directly proportional to this source term. Fig. 10 provides an insight on the impact of this unknown parameter by presenting the variation of fluoride release with a 20% variation of the input source term. As shown by the figure, the obtained fluoride release rate is quite directly proportional to the variation of the Fe^{2+} source term. Its value has thus been fitted to obtain a good agreement with the experimental results at 353 K. A temperature dependent source term of Fe^{2+} can help adjust the level of degradation between several temperatures, while a current dependent one can adjust the degradation form along current density. In order to give an illustration, Fluoride release results obtained with three different Fe^{2+} source terms are presented in Fig. 13. As can be seen, the choice of one source term compared to another does not modify the overall behavior of the fluoride release rate with current density but can significantly change the position of the peak and the magnitude at one temperature compared with another. The law that gives the best results is the temperature dependent one (last result on Fig. 13). With this laws, we capture the right peak position and magnitude at 353 K and the right peak position at 333 K, while the fluoride release at low current densities at 333 K is slightly overestimated. This law will be used to model the time evolution of the membrane thickness in the next section.

Membrane thinning

In the two previous sections, a 1D PEMWE model that incorporates chemical degradation of the membrane has been developed and validated against experimental data. The objective of this section is to deduce from this physical model, the time evolution of the membrane thickness. Indeed, as the membrane thins down, oxygen crossover increases, which accelerates the Fluor release rate and the membrane degradation and thus accelerates the thinning of the membrane. The time evolution of the membrane thickness is thus expected not to be linear but exponential. Modeling the thinning

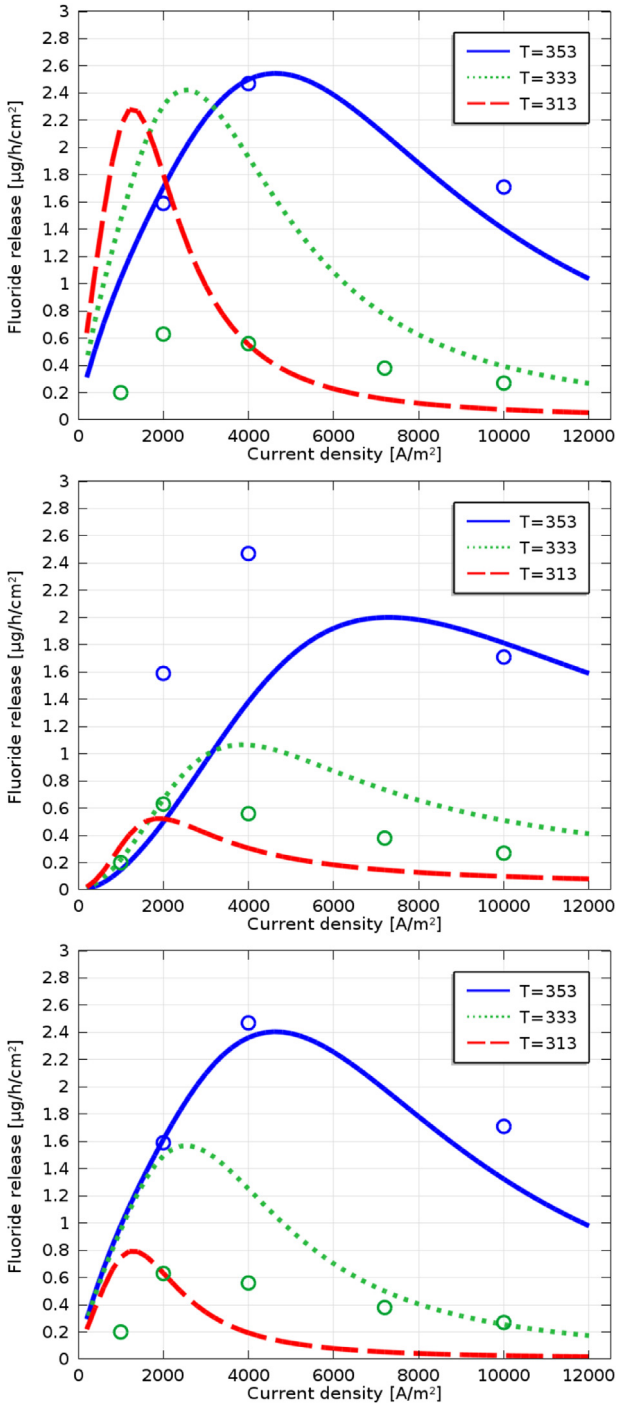

Fig. 13 – Fluoride release at 313, 333 and 353 K in µg/h/cm² with comparison to experimental points. Top: Constant source term of Fe^{2+} ions fitted to 9×10^{-2} mol/m³/s. Middle: Imposed inlet concentration of Fe^{2+} ions fitted to 3 ppm. Bottom: Temperature dependent source term of Fe^{2+} ions using Equation (34), the source term at 353 K being equal to 9×10^{-2} mol/m³/s.

of the membrane implies changes in geometry. To work around this difficulty, a change of variable on the spatial variable x, which corresponds to the direction of the membrane thickness, is performed:

$$x' = \frac{e_M}{e_M^0} x \tag{35}$$

where e_M^0 is the thickness of the membrane at time zero. By doing this change of variable, some physical constants within the membrane become time-dependent (the ionic conductivity, the diffusion coefficients and the water velocity), but the rest of the model is not modified:

$$\kappa' = \left(\frac{e_M}{e_M^0}\right)^2 \kappa \tag{36}$$

$$D_i' = \left(\frac{e_M}{e_M^0}\right)^2 D_i \tag{37}$$

$$v_{H_2O}' = \frac{e_M}{e_M^0} v_{H_2O} \tag{38}$$

The time evolution of the thickness of the membrane is modeled in the following way:

$$\frac{de_M}{dt} = \Delta e_M R_{fluor} \tag{39}$$

where Δe_M corresponds to the thinning of the membrane per mol of released fluor and R_{fluor} is the Fluor release in mol/s, obtained from the degradation membrane model.

Fig. 14 gives the time evolution of the membrane thickness in percentage of its initial value when operating at 1 A cm^{-2} at 333 K and 353 K. As expected, the life time is significantly decreased at high temperature. The time needed to thin 50% of the membrane is around 38′500 h at 333 K but only 8′700 h at 353 K. The evolution shows the coupling effect which leads to a non-linear decrease of the membrane thickness. The coupling effect accelerates the membrane degradation. To visualize this effect, the membrane thickness time evolution obtained using for the Fluor release rate a constant value (the one obtained at time zero) is also displayed Fig. 14. Using the linear model, the time needed to thin 50% of the membrane is 59′500 h at 333 K and

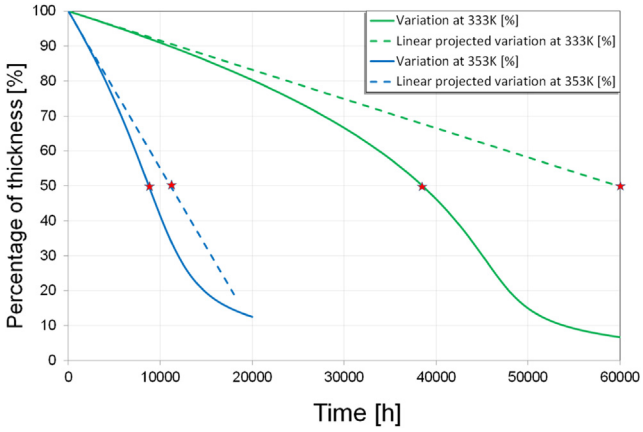

Fig. 14 – Time evolution of the membrane thickness in percentage at 1 A cm^{-2} at 333 K and 353 K. Plain lines: coupled model taking into account the thinning of the membrane; dotted lines: linear model without the coupling with the membrane thinning.

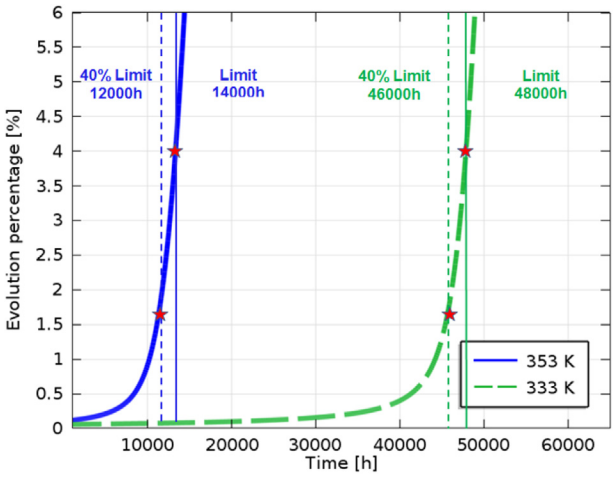

Fig. 15 – Time evolution of the molar percentage of H_2 at the anode at 333 K and 353 K.

11′100 h at 353 K. Without taking into account the coupling effect, the life-time expectation of the electrolyzer is overestimated by 57% at 333 K and 27% at 353 K.

After roughly 50′000 and 12′000 h respectively, it can be observed (Fig. 14) that the membrane thickness decrease presents a deceleration. This is attributed to the fact that at these moments, the oxygen and hydrogen cross-over present an exponential increase and thus the parasitic reaction 6 increases strongly leading to an increased consumption of the free radicals and thus a deceleration of the attack of the membrane. Nevertheless, these data should not be taken into account as the explosivity limit has been reached. Indeed, an important criterion for the electrolyzer is the molar percentage of H_2 in O_2, as this mixture becomes explosive above 4% of H_2 in O_2 Ref. [39]. Fig. 15 plots the evolution of this quantity at 333 and 353 K. An exponential increase is observed due to the coupling between the thinning of the membrane leading to the gas cross-over increase and the chemical degradation of the membrane. This trend is completely similar to the one observed experimentally by Inaba et al. [40] when performing accelerated stress test in PEMFC.

Conclusions

This work focuses on membrane degradation in PEM water electrolyzer and more precisely on the impact of temperature and current density on the chemical degradation rate. The chemical degradation rate has been characterized by regularly collecting the effluent water of the cell at the anode and at the cathode sides and by measuring the fluoride release rate in the samples with a fluoride selective electrode. Membrane degradation occurs mainly at the cathode side. Increasing the temperature increases strongly the membrane chemical degradation. Regarding the current density, the effect is smaller and more complex. At very low current density, the degradation rate is low, then it increases as the current density increases to reach a maximum at quite low current density and then decreases.

To understand this behavior, a 1D polymer electrolyte membrane water electrolyzer (PEMWE) model that incorporates chemical degradation of the membrane has been developed. The chemical membrane degradation mechanisms are the oxygen cross-over from the anode to the cathode side, the formation of hydrogen peroxyde at the cathode side together with the subsequent formation of radicals via Fenton reactions involving metal-ion impurities and the membrane degradation. With these developments, the model is able to capture the temperature and current density effects on the degradation rates. In particular, the maximum degradation rate at quite low current density is captured and has been analyzed. The decrease in the degradation rate at high current densities was expected since when increasing the current density the molar percentage of oxygen at the cathode decreases and thus the formation of peroxyde and free radicals. At low current density, the observed behavior was not expected but is well explained by the model. It is due to the competition between two reactions that consume the $HO^{\bullet}$ radicals: a reaction that involves peroxyde and the reaction leading to the membrane attack. At low current density, peroxyde concentration is quite high. The reaction that involves peroxyde becomes predominant leading to a decrease in the degradation rate.

Finally, the model has been used to study the time evolution of the membrane thickness when applying a constant current density. The model is able to capture the acceleration of the degradation, which can be also seen though an exponential increase of the gas cross-over. In the future, we plan to use this model to study the impact of different current density profiles on the membrane thinning and thus on the expected life-time of the electrolyzer under dynamic conditions.

Acknowledgments

This work has been performed within the European project NOVEL. The financial support of the European 7th Framework Programme (Grant Agreement 303484) and of CEA is gratefully acknowledged.

REFERENCES

[1] Barbir F. PEM electrolysis for production of hydrogen from renewable energy sources. Sol Energy 2005;78:661–9.
[2] Millet P, Ngameni R, Grigoriev SA, Mbemba N, Brisset F, Ranjbari A, et al. PEM water electrolyzers: from electrocatalysis to stack development. Int J Hydrogen Energy 2010;35:5043–52. http://dx.doi.org/10.1016/j.ijhydene.2009.09.015.
[3] Millet P, Ngameni R, Grigoriev S, Fateev V. Scientific and engineering issues related to PEM technology: water electrolysers, fuel cells and ununiti regenerative systems. Int J Hydrogen Energy 2011a;36:4156–63.
[4] Millet P, Mbemba N, Grigoriev S, Fateev V, Aukauloo A, Etievant C. Electrochemical performances of PEM water electrolysis cells and perspectives. Int J Hydrogen Energy 2011b;36:4134–42.
[5] Choi P, Bessarabov DG, Datta R. A simple model for solid polymer electrolyte (SPE) water electrolysis. Solid State

Ionics 2004;175:535–9. http://dx.doi.org/10.1016/j.ssi.2004.01.076.
[6] Biaku C, Dale NV, Mann MD, Salehfar H, Peters A, Han T. A semiempirical study of the temperature dependence of the anode charge transfer coefficient of a 6 kW PEM electrolyzer. Int J Hydrogen Energy 2008;33:4247–54. http://dx.doi.org/10.1016/j.ijhydene.2008.06.006.
[7] Dale NV, Mann MD, Salehfar H. Semiempirical model based on thermodynamic principles for determining 6 kWproton exchange membrane electrolyzer stack characteristics. J Power Sources 2008;185:1348–53. http://dx.doi.org/10.1016/j.jpowsour.2008.08.054.
[8] Awasthi A, Scott K, Basu S. Dynamic modeling and simulation of a proton exchange membrane electrolyzer for hydrogen production. Int J Hydrogen Energy 2011;36(22):14779–86. http://dx.doi.org/10.1016/j.ijhydene.2011.03.045.
[9] Garcia-Valverde R, Espinosa N, Urbina A. Simple PEM water electrolyser model and experimental validation. Int J Hydrogen Energy 2011;37(2):1927–38. http://dx.doi.org/10.1016/j.ijhydene.2011.09.027.
[10] Marangio F, Santarelli M, Cali M. Theoretical model and experimental analysis of a high pressure PEM water electrolyzer for hydrogen production. Int J Hydrogen Energy 2009;34:1143–58.
[11] Grigoriev S, Millet P, Volobuev S, Fateev V. Optimization of porous current collectors for PEM water electrolysers. ISSN 0360–3199 Int J Hydrogen Energy 2009;34(11):4968–73. http://dx.doi.org/10.1016/j.ijhydene.2008.11.056. 2nd International Workshop on Hydrogen, 2nd International Workshop on Hydrogen.
[12] Franco AA, Guinard M, Barthe B, Lemaire O. Impact of carbon monoxide on PEFC catalyst carbon support degradation under current-cycled operating conditions. Electrochim Acta 2009;54:5267–79.
[13] Franco AA, Gerard M. Multiscale model of carbon corrosion in a PEFC: coupling with electrocatalysis and impact on performance degradation. J Electrochem Soc 2008;155(4):B367–84. http://dx.doi.org/10.1149/1.2838165.
[14] Shah A, Ralph T, Walsh F. Modeling and simulation of the degradation of Perfluorinated ion-exchange membranes in PEM fuel cells. J Electrochem Soc 2009;156:B465–84. http://dx.doi.org/10.1149/1.3077573.
[15] Wong KH, Kjeang E. Macroscopic in-situ modeling of chemical membrane degradation in polymer electrolyte fuel cells. J Electrochem. Soc 2014;161(9):F823–32.
[16] Riascos LAM, Pereira D. Limit operating temperature in polymer electrolyte membrane fuel cells. J Electrochem Soc 2009;156(9):B1051–8.
[17] LaConti AB, Liu H, Mittelsteadt C, McDonald R. Polymer electrolyte membrane degradation mechanisms in fuel cells. Findings over the past 30 years and comparison with electrolyzers. ECS Trans 2006;1(8):199–219.
[18] Lampinen MJ, Fomino M. Analysis of free energy and entropy changes for half-cell reactions. J Electrochem Soc 1993;140(12):3537–46. http://dx.doi.org/10.1149/1.2221123.
[19] Springer TE, Zawodzinski TA, Gottesfeld S. Polymer electrolyte fuel cell model. J Electrochem Soc 1991;138(8):2334–42. http://dx.doi.org/10.1149/1.2085971.
[20] Ito H, Maeda T, Nakano A, Takenada H. Properties of Nafion membranes under PEM water electrolysis conditions. Int J Hydrogen Energy 2011;36:10527–40.
[21] Ito H, Maeda T, Nakano A, Kato A, Yoshida T. Influence of pore structural properties of current collectors on the performance of proton exchange membrane electrolyzer. Electrochim Acta 2013;100:242–8.
[22] Rozain C. Développement de nouveaux matériaux d'électrodes pour la production d'hydrogène par électrolyse de l'eau [Ph.D. thesis]. Université Paris-sud XI; 2013.
[23] Coulon R, Bessler WG, Franco A. Modeling chemical degradation of a polymer electrolyte membrane and its impact on fuel cell performance. ECS Trans 2010;25:259.
[24] Collier A, Wang H, Yuan XZ, Zhang J, Wilkinson DP. Degradation of polymer electrolyte membranes. ISSN 0360–3199 Int J Hydrogen Energy 2006;31(13):1838–54. http://dx.doi.org/10.1016/j.ijhydene.2006.05.006.
[25] Stucki S, Scherer GG, Schlagowski S, Fischer E. PEM water electrolysers: evidence for membrane failure in 100 kW demonstration plants. J Appl Electrochem 1998;28:1041–9.
[26] Ogumi Z, Takehara Z, Yoshizawa S. Gas permeation in SPE method. J Electrochem Soc 1984;131:769–73.
[27] Mann R, Amphlett J, Peppley B, Thurgood C. Application of Butler–Volmer equations in the modelling of activation polarization for PEM fuel cells. J Power Sources 2006;161:775–81.
[28] Bernardi DM, Verbrugge MW. A mathematical model of the solid-polymer-electrolyte fuel cell. J Electrochem Soc 1992;139(9):2477–91. http://dx.doi.org/10.1149/1.2221251.
[29] Amphlett J, Baumert R, Mann R, Peppley B, Roberge P, Harris T. Performance modeling of the ballard mark IV solid polymer electrolyte fuel cell. J Electrochem Soc 1995;142(1):9–15. http://dx.doi.org/10.1149/1.2043866.
[30] Parthasarathy A, Srinivasan S, Appleby AJ. Temperature dependence of the electrode kinetics of oxygen reduction at the platinum/nation interface – a microelectrode investigation. J Electrochem Soc 1992;139:2530–7.
[31] Wise DL, Houghton G. The diffusion coefficients of ten slightly soluble gases in water at 10–60 °C. Chem Eng Sci 1966;21:999–1010.
[32] Ruvinskiy PS, Bonnefont A, Pham-Huu C, Savinova ER. Using ordered nanomaterials for shedding light on the mechanism of the cathodic oxygen reduction reaction. Am Chem Soc 2011;27:9018–27.
[33] Sethuraman V, Weidner J, Haug A, Motupally A, Protsailo L. Hydrogen peroxyde formation rrate in a PEMFC anode and cathode. Effect of humidity and temperature. J Electrochem Soc 2008;155(1):B50–7.
[34] Anderson A, Albu T. Catalytic effect of platinum on oxygen reduction. An Ab initio model including electrode potential dependence. J Electrochem Soc 2000;147(11):4229–38.
[35] Gubler L, Dockheer S, Koppenal H. Radical (HO, H and HOO) formation and ionomer degradation in polymer electrolyte fuel cells. J Electrochem Soc 2011;158(7):B755–69.
[36] Rigg T, Taylor W, W. J. The rate constant of the reaction between hydrogen peroxyde and ferrous ions. J Chem Phys 1954;22(4):575.
[37] Feng K, Wu G, Li Z, Cai X, Chu P. Corrosion behavior of SS316L in simulated and accelerated PEMFC environments. Int J Hydrogen Energy 2011;36:13032–42.
[38] Yang Y, Guo L, Liu H. Factors affecting corrosion behavior of SS316L as bipolar plate material in PEMFC cathode environments. Int J Hydrogen Energy 2012;37:13822–8.
[39] Schroeder V, Holtappels K. Explosion characteristics of hydrogen-air and hydrogen–oxygen mixtures at elevated pressures. Pisa, Italy: First ICHS; 2005.
[40] Inaba M, Kinumoto T, Kiriake A, Umebayashi R, Tasaka A, Ogumi Z. Gas crossover and membrane degradation in polymer electrolyte fuel cells. Electrochem Acta 2006;51:5746–53. http://dx.doi.org/10.1016/j.electacta.2006.03.008.